

A New Generation of Adsorbent Materials for Entrapping and Immobilizing Highly Mobile Radionuclides

Yifeng Wang, Huizhen Gao,
Andy Miller and Phillip Pohl
*Sandia National Laboratories
USA*

1. Introduction

The United States is now re-assessing its nuclear waste disposal policy and re-evaluating the option of moving away from the current once-through open fuel cycle to a closed fuel cycle. In a closed fuel cycle, used fuels will be reprocessed and useful components such as uranium or transuranics will be recovered for reuse (e.g., Bodansky, 2006). During this process, a variety of waste streams will be generated (NEA, 2006; Gombert, 2007). Immobilizing these waste streams into appropriate waste forms for either interim storage or long-term disposal is technically challenging (Peters and Ewing, 2007; Gombert, 2007). Highly volatile or soluble radionuclides such as iodine (^{129}I) and technetium (^{99}Tc) are particularly problematic, because both have long half-lives and can exist as gaseous or anionic species that are highly soluble and poorly sorbed by natural materials (Wang et al., 2003; Wang and Gao, 2006; Wang et al., 2007). Waste forms are probably the only engineered barrier to limit their release into a human-accessible environment after disposal. In addition, during the fuel reprocessing, a major fraction of volatile radionuclides will enter the gas phase and must be captured in the off-gas treatment. It is thus highly desirable to develop a material that can effectively capture these radionuclides and then be converted into a durable waste form.

In fuel reprocessing, spent fuels are first subjected to voloxidation and acid dissolution, during which 94% to 99% of iodine-129, together with other volatile radionuclides (^{14}C , ^3H , Kr and Xe), are released to the off-gas stream (Gombert, 2007). Various methods have been proposed for the recovery of volatile ^{129}I , including scrubbing with caustic or acid solutions and chemisorption on impregnated adsorbents (Rovnyi et al., 2002; Kato et al., 2002; Gombert, 2007). The proposed adsorbents include both natural and artificial porous materials like zeolite (e.g., mordenite), alumina, and silica gels loaded with metals (e.g., Ag, Cd, Pb) that form low-solubility iodides or iodates. However, several issues have been recognized regarding the effectiveness of these materials (Gombert, 2007). For example, based on adsorption models, iodine diffusion inside the zeolite particles was found to be slow, only about 2×10^{-14} cm^2/s , and likely to limit the adsorption process (Jubin, 1994, Gombert, 2007). The stability of silver-exchanged zeolite is also a concern. For example,

silver-exchanged faujasite (AgX) decomposes in the presence of NO_x and water vapor. AgX also does not exhibit satisfactory thermal stability during regeneration. In addition, the fibrous nature of mordenite may present an inhalation hazard (Stephenson et al., 1999). Silver-impregnated alumina and silica capture iodine by forming AgI along grain boundaries. The high iodine leaching rate of these materials can be a potential issue if they are directly used for disposal. Currently, no path forward has been established for the disposition of these adsorbent materials. In addition, metal-organic frameworks (MOFs) have been found to have high sorption capacities and are tunable to different volatile elements (Sudik et al., 2006; Lee et al., 2007). However, the long term fate of the organic structure in a high heat/radiation field is unknown.

In this chapter, we present a new concept for the development of a next generation of high-performance radionuclide adsorbent materials for nuclear waste reprocessing and disposal. Based on this new concept, we have developed a suite of inorganic nanocomposite materials (SNL-NCP) that can effectively entrap various radionuclides including gaseous ^{129}I and anionic ^{99}Tc . Importantly, after the sorption of radionuclides, these materials can be easily converted into nanostructured waste forms, which are expected to have unprecedented flexibility to accommodate a wide range of radionuclides with high waste loadings and low leaching rates.

2. Nano-scale radionuclide immobilization and encapsulation

The development of SNL-NCP materials are based on the concept of nano-scale radionuclide immobilization and encapsulation (Fig. 1). For example, for capture of iodine, a nanoporous material that has a high sorption capability for iodine gas is first synthesized. The sorption capability can be further improved, as needed, through pore surface modification. The material is then used as an adsorbent to entrap gaseous iodine. The entrapped iodine is converted to a less volatile compound, for example, by reacting with silver to form AgI precipitates inside nanopores of the material. The iodine-loaded material is finally mixed with glass-forming constituents and calcined, resulting in a waste form in which I-bearing nanoparticles are embedded in a glass or crystalline matrix. More recent development of this technology allows us to avoid using Ag or other heavy metals for iodine immobilization and subsequent vitrification (see Section 5 of this chapter).

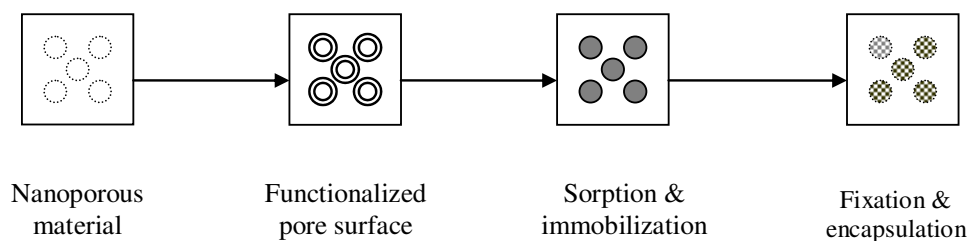


Fig. 1. Formation of a nanocomposite waste form. In the final waste form, nano-scale radionuclide precipitates are embedded in a glass or ceramic matrix.

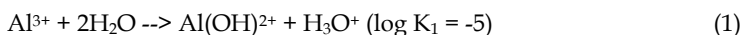
Existing waste forms tend to incorporate radionuclides into rigid crystal structures (e.g., Xu and Wang, 2000; Fortner et al., 2002; Ewing, 2006; Grambow, 2006), and the waste loading of those materials is generally limited by various structural factors such as the size and charge of a target radionuclide. Unlike the existing waste forms, the new waste forms we developed incorporate radionuclides as nano-scale inclusions in a host matrix and thus effectively relax the constraint of crystal structure on waste loadings. Therefore, the new waste forms are able to accommodate a wide spectrum of radionuclides with high waste loadings and low leaching rates. Since the leaching rates are controlled by the dissolution rate of the host mineral, it is even possible to engineer a waste form that will be thermo-dynamically stable in a repository environment, by choosing an appropriate host mineral. A good analog to this is the naturally occurring nano-scale fluid inclusions in mineral crystals, which remain intact over millions of years (Wang et., 2003). It is anticipated that SNL-NCP materials can be easily integrated into the fuel reprocessing system currently proposed for advanced fuel cycles.

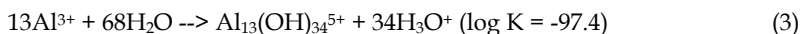
3. Synthesis of nanoporous metal oxides

More than 300 nanoporous metal oxide materials have been synthesized with a sol-gel route developed specifically for this work. In this route, inorganic metal salts are used as precursors, a block copolymer as a nanostructural template, and an epoxy (propylene oxide in this case) as a proton scavenger. The synthesis can be conducted under relatively simple ambient conditions from room temperature to 65 °C. A nanoporous metal oxide is obtained by drying the resultant gel at 80 °C and calcining it at or below 600 °C in air or oxygen atmosphere. Since it uses inexpensive inorganic precursors, the synthesis route we developed can be scaled up for a large quantity of production if needed.

For example nanoporous alumina can be synthesized with the following chemicals and procedure. The chemicals used for the this synthesis include: aluminum chloride hexahydrate ($\text{AlCl}_3 \cdot 6\text{H}_2\text{O}$, e.g., from Fisher), propylene oxide ($\text{C}_3\text{H}_6\text{O}$, PO, e.g., from Fisher), poly(ethylene glycol)-block-poly(propylene glycol)-block-poly(ethylene glycol) (P123, e.g., from Aldrich, $M_n=5800$), and anhydrous alcohol (e.g., from Fisher Acros). For solution A, 12 grams of P123 are dissolved in 72 mL alcohol (anhydrous). For solution B, 34 g of $\text{AlCl}_3 \cdot 6\text{H}_2\text{O}$ is dissolved in 90 mL of a $\text{H}_2\text{O}/\text{C}_2\text{H}_5\text{OH}$ (1:1) mixture. A typical synthesis process involves mixing the two prepared homogeneous solutions (A and B) until the solids dissolve, then combining them into a single parent solution. To this parent solution, 47 g of propylene oxide is added. This precipitates the alumina which is then aged at room temperature in the hood for about 3 days, and then dried at about 80°C in the oven for about 24 hours to turn it into a gel. The gel is finally calcined at 600°C for about 4 hours at a temperature ramp of about 5°C/min.

The involvement of a structural directing agent and the control of the polymerization rate of alumina hydroxides are two important factors for this synthesis. Block copolymer P123 (or other copolymer) is used as a template for nanostructures. The polymerization rate is controlled by adding a certain amount of propylene oxide (or ethylene oxide or other epoxy) to solution B. Aluminum ion, Al^{3+} , in solution has a great tendency to form positively charged polynuclear species (hydroxoaluminum complex) as follows:





Propylene oxide in the solution acts as a proton scavenger by the nucleophilic reaction towards ring-opening. This reaction is irreversible and slow, thus maintaining a uniform pH gradient in the solution for hydrolyzing the aluminum salt.

The synthesis route has also been adapted to one-pot syntheses of nanoporous materials containing multiple metal components (e.g., Ag-Al, Ni-Al, or Bi-Al oxides). This one-pot process allows us to ensure the chemical and structural homogeneity of synthesized composite material. A nanoporous Ni-Al oxide material obtained using this route is shown in Figure 2. The structural homogeneity of this material is confirmed with transmission electron microscopic (TEM) observations.

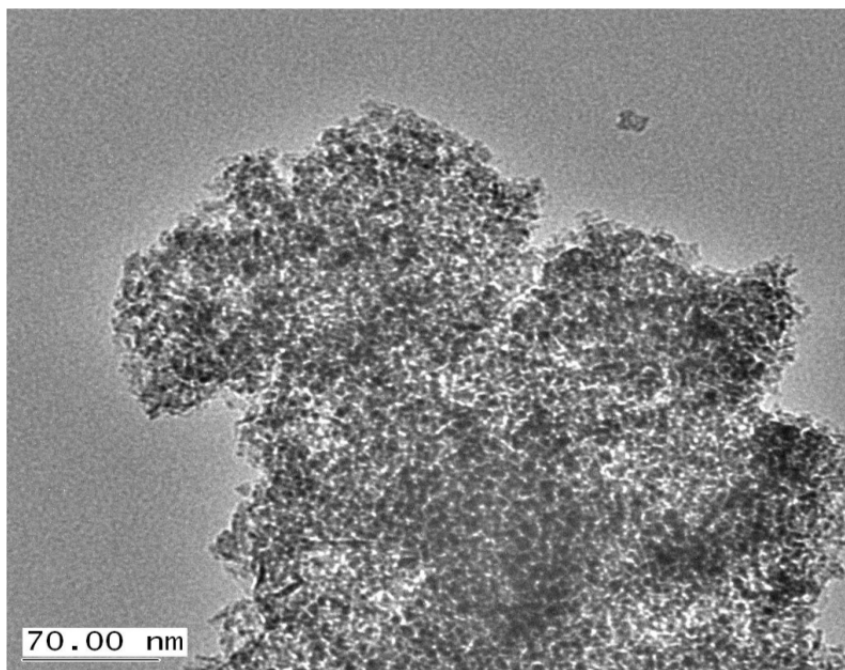


Fig. 2. Transmission Electron Microscopic (TEM) image of nanoporous Ni-Al oxides, showing worm-like nanopore structures.

The synthesized materials have been characterized with a powder x-ray diffractometer (XRD, Burker D8 Advance), surface area and porosity analyzer (BET TriStar 3000, Micromeritics), and transmission electron microscope (TEM, Jeol). The XRD analyses generally indicate that the synthesized materials have low crystallinity. The BET measurements show that these materials have pore sizes ranging from 11 to 16 nanometers and surface areas from 320 to 450 m²/g (see Table 1, Fig. 3).

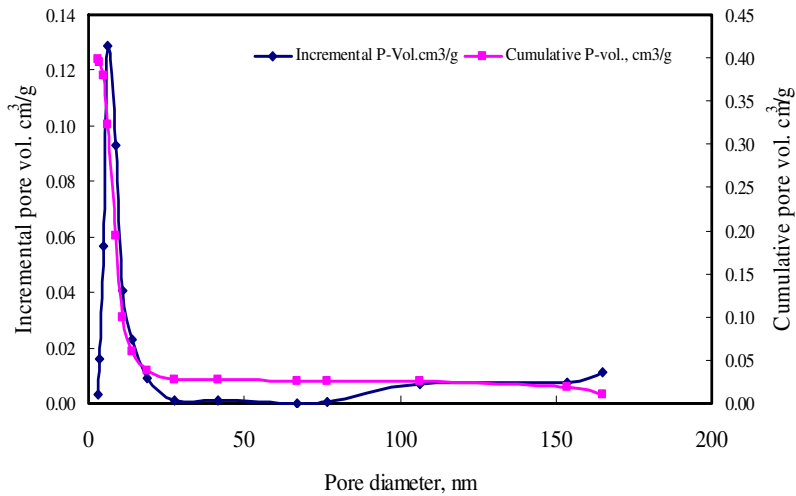


Fig. 3. Pore size distribution of Ni-Al (Ni:Al = 1:1) nanoporous material determined from BET measurements.

Sample ID	Single point surface area, m ² /g	Pore volume, cm ³ /g Single point (ads.)	Pore size, nm (Ads. Average)
Nanoporous-alumina (commercial)	263.63	0.49	7.21
NC 13-A-600C/air	415.83	1.53	14.69
NC 13-A400C/O ₂	447.25	1.35	11.87
NC 13-B-600C/air	336.90	1.38	15.78
NC20-1 (m-Al batch 4)	319.35	1.13	13.65

Table 1. BET surface area, pore volume, and pore size of synthesized nanoporous alumina

4. Radionuclide sorption on nanoporous metal oxides

A set of SNL-NCP and other related materials were selected and tested for the sorption of gaseous iodine under simulated fuel reprocessing conditions. These tests provide important information regarding the selectivity of materials for iodine sorption and the potential interference of other chemical components anticipated to be present in off-gas waste stream from fuel reprocessing.

The tests were performed under elevated temperature (90°C) and variable relative humidity conditions, as well as with or without CO₂ and NO₂ gas added in the headspace. The general experimental setup for iodine sorption testing is shown in Figure 4. The Tc sorption capabilities were determined with batch experiments using Re as a chemical analog for Tc. The materials tested for iodine sorption include various SNL-NCP materials (NC-77), Al-Mg layered double hydroxides (NC-88) calcined at different temperatures, mesoporous silica, activated alumina (particles), sepiolite, palygorskite, and zeolite. These materials, all inorganic, encompass diverse chemical compositions and mineral structures and thus help to mechanistically understand iodine sorption on SNL NCP materials. After each iodine sorption test, the sorbent was mixed with SiO₂ and iodine concentrations in the adsorbent were measured with an ARL QUANT'X Energy-Dispersive X-Ray Fluorescence (EDXRF) Spectrometer (Thermo Electron Corporation).

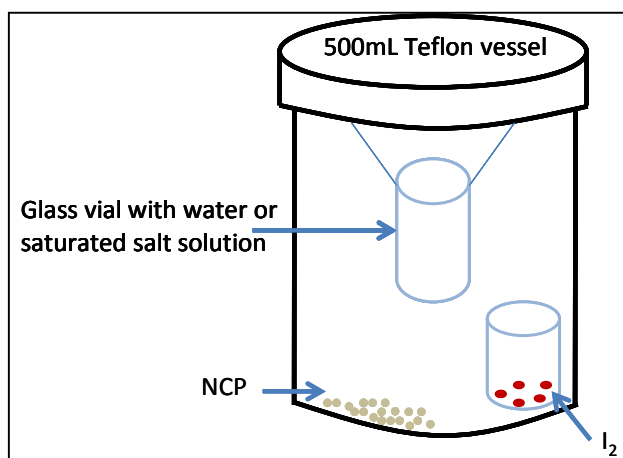


Fig. 4. Experimental setup for testing iodine sorption under various relative humidity conditions. The relative humidity inside the glass vial is controlled by a saturated salt solution.

Selected results of the batch sorption experiments are shown in Table 2. All these materials have exhibited high sorption capabilities for I₂ gas and TcO₄⁻ ion. A typical iodine sorption isotherm is shown in Figure 5. The data were obtained from exhaustion experiments, in which the iodine-loaded material was heated overnight at about 90 °C and cooled to about room temperature in an open jar. The change in the slope of the isotherm may reflect the transition from monolayer sorption to multi-layer sorption and eventually to pore condensation as the mass ratio of iodine to adsorbent increases. It was found that I sorbed in the Ni-Al material forms a separate Ni-Al-I phase in the nanopores, which may be responsible for the high I sorption capability observed. This leads to the possibility of using Ni or other metals, rather than relatively expensive Ag, for immobilizing I in a final waste form.

Materials	Specific surface area (m ² /g)	Pore size (nm)	Target radionuclides	Sorption capability
Alumina (Al ₂ O ₃)	300-450	12-14	I	[I] = 2 - 4x10 ³ ppm
Ag-Al oxide	200	6.5	I	[I] = 1.9-4.0x10 ⁴ ppm
Ni-Al oxide	260	7	I, Tc*	[I]=2x10 ⁴ ppm K _d =210 mL/g for Re
Bi-Al oxide	160	7	I, Tc*	K _d =1680 mL/g for Re

*Rhenium is used as the surrogate of Tc.

Table 2. Sorption capability of nanoporous metal oxides for iodine and technetium

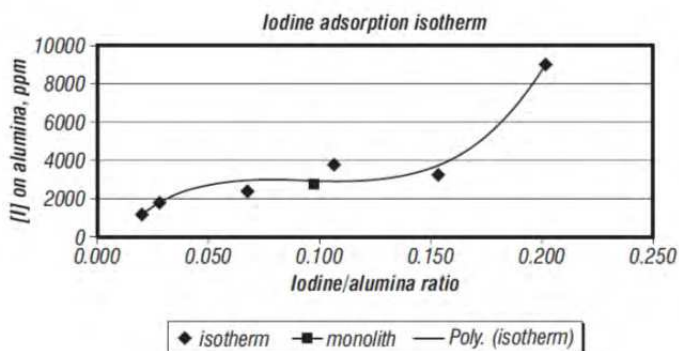


Fig. 5. Isotherm of iodine adsorption on nanoporous alumina. Measurements were made after overnight desorption at 90°C following adsorption

The experimental testing has confirmed that nanoporous Al oxide and its derivatives have high sorption capabilities for iodine sorption. To understand the underlying mechanism, the same sorption experiment was performed on nanoporous silica, which has a larger surface area and a smaller pore sizes than the alumina materials. Interestingly, no significant I sorption was observed on the silica material, implying that the surface chemical identity of the material plays an important role in I sorption. On the other hand, we have found that nanoporous structures can greatly enhance I sorption onto alumina. These observations lead us to conclude that the high I sorption capabilities of nanoporous alumina and its derivatives are attributed to the combined effects of surface chemistry and nanopore confinement. This points to a possibility of optimizing material performance for sorption capability and selectivity by manipulating material compositions and structures.

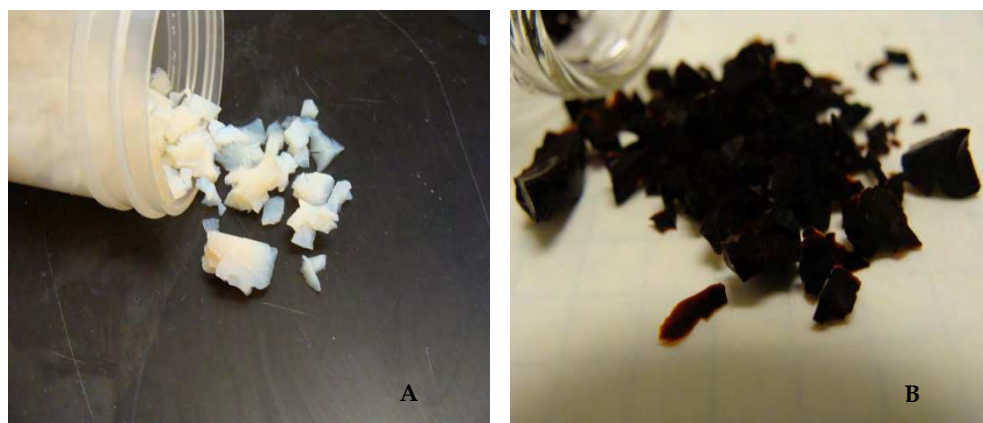


Fig. 6. Formation of monolithic nanoporous SNL-NCP-A. A - before I sorption; B - after I sorption. Each individual grain has nanoporous structures. The dark brown color in B indicates that the monolithic material has a high I sorption capability. The size of monolithic grains ranges from mm to cm.

SNL-NCP materials can also be engineered into monolithic forms (Fig. 6). Monolithic materials are generally preferred for engineering handling. As shown in Table 3, a monolithic form of SNL-NCP has an iodine sorption capability as high as the corresponding powder, indicating molecular diffusion in nanopores is not a limiting step for adsorption. Also, note that monolithic nanoporous alumina without silver incorporated has at least the same comparable iodine sorption capability as the nanoporous alumina with Ag included. Therefore, Ag may not be needed for I sequestration if nanoporous alumina is used as a getter material. Our experiments also show that zeolite materials have a low sorption capability for iodine, indicating that that zeolite component itself does not contribute much to the iodine sorption capability of Ag-exchanged zeolite materials and thus casting doubt on the necessity of using zeolite as a supporting material for iodine capture.

Material	I/(m-Al) ratio	Sample wt, g	[I] uptake, ppm	
Nanoporous alumina w/ Ag	0.114	0.2036	35674	
Monolithic Nanoporous alumina w/o Ag	0.107	0.2035	66245	
BET measurements				
Material	Surface area, m ² /g	Pore vol. cm ³ /g	Pore size, nm	Micropore vol. cm ³ /g
Nanoporous alumina w/ Ag	215	0.706	12.7	0.006644
Monolithic Nanoporous alumina w/o Ag	354	1.75	19.15	0.014549

Table 3. Iodine sorption on nanoporous alumina and its derivatives

The experimental setup for iodine sorption tests under a controlled relative humidity is shown in Figure 4. The relative humidity (RH) in the headspace was controlled by the presence of a saturated salt solution in the test vessel. The salt solutions used include: LiCl - RH 10.23%, MgCl₂ - 24.12%, KCl - 78.5%, and deionized water (DI) - 100%. The testing results are shown in Figure 7. Nanoporous materials NC-77 and NC77-N2 outperform most of the other materials tested over the whole relative humidity range. SNL-NCP materials are relatively insensitive to water interference for iodine sorption. This unique property is important for the potential use of SNL-NCP materials as an iodine scavenger in the off-gas treatment during fuel reprocessing. Two layered double hydroxide materials NC88-380 and NC88-600, which can be considered as nanostructured layered materials, also exhibit high iodine sorption capabilities under high relative humidity. Sepiolite and palygorskite are two naturally occurring silicate materials with similar tunnel structures and slightly different chemical compositions. The two materials, however, display distinct sorption behaviors. Particularly, sepiolite is very sensitive to water vapor, even though its sorption capability for iodine is high at zero relative humidity. This is because sepiolite generally has a high affinity for polar molecules such as H₂O. Mesoporous silica has a relatively lower iodine sorption capability as compared with SNL-NCP materials with a similar nanoporous structure, again indicating the surface chemical identity of the material plays an important role in iodine sorption. It is interesting to note that zeolite has a relatively low sorption capability for iodine over the whole range of relative humidity.

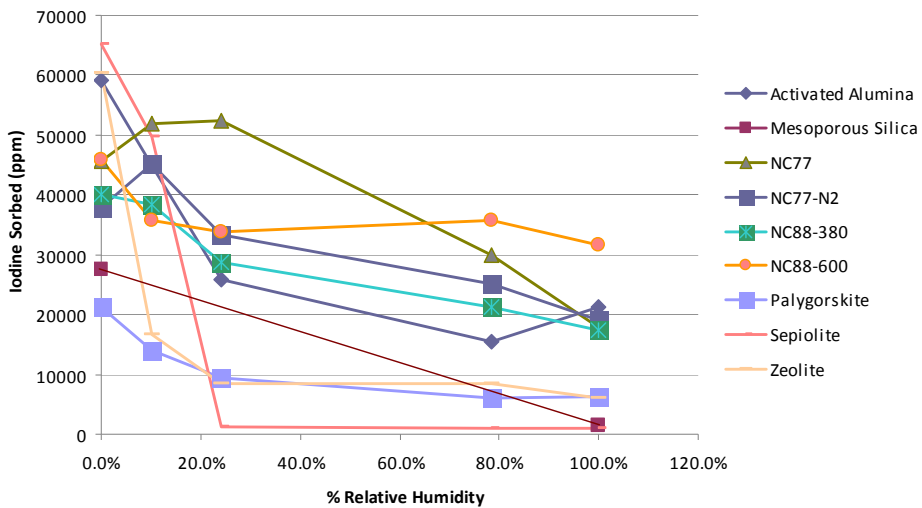


Fig. 7. Iodine sorption onto SNL-NCP and other related materials under variable relative humidity

5. Radionuclide fixation and encapsulation

A suite of techniques have been developed for the fixation of radionuclides in metal oxide nanopores. The key to this fixation is to chemically convert a target radionuclide into a less volatile or soluble form. Iodine can be fixed in two ways: (1) introducing Ag to a getter material to convert I_2 into AgI upon sorption and (2) adding a chemical base (e.g., Na_4SiO_4) to an I_2 -loaded material to convert I_2 to iodide or iodate ions. X-ray photoelectron spectra (XPS) show that 66% of I_2 is converted to I⁻ upon iodine sorption onto Ag-alumina nanoporous material (Fig. 8). Similarly, Fourier Transformation Infrared spectroscopic (FTIR) analysis indicates that adding Na_4SiO_4 during I fixation forces the sorbed iodine gas in the nanopores to completely convert to I⁻ and IO_3^- , thus significantly reducing iodine volatility. The second approach is preferred for I fixation, because it avoids using silver. We have found that the same method may also apply to Tc fixation. Preliminary data indicate that addition of Na_4SiO_4 or NaOH helps convert TcO_4^- into insoluble TcO_2 . The detailed mechanism for this conversion still needs to be clarified.

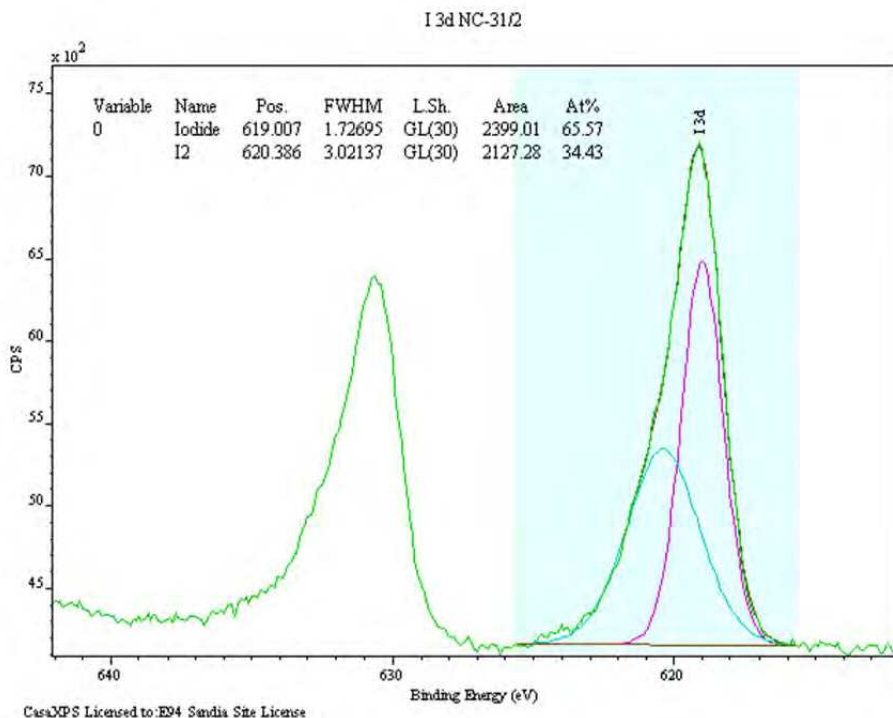


Fig. 8. X-ray photoelectron spectra (XPS) showing 66% of I_2 converted to I⁻ upon iodine sorption onto Ag-alumina nanoporous material.

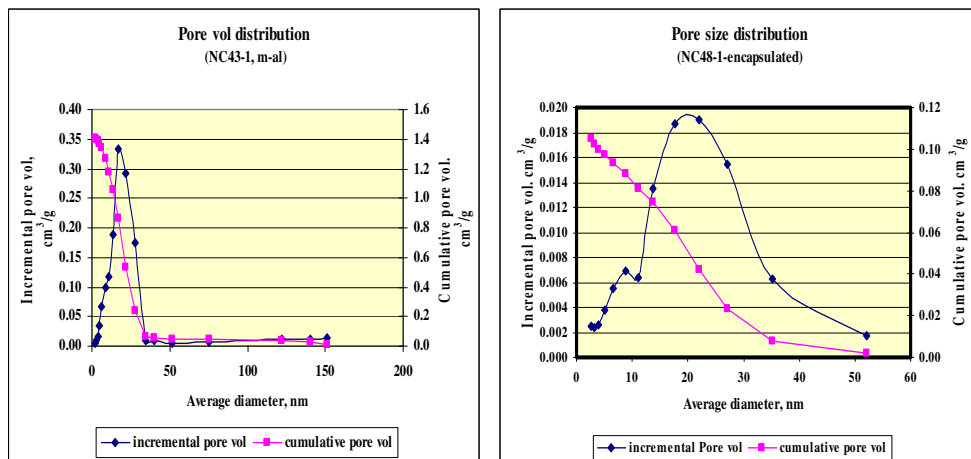


Fig. 9. Effective sealing of nanopores with Na-silicate solution. Left – pore volume distribution before sealing; Right - pore volume distribution after sealing. Note the changing y-axis values.

Radionuclides loaded onto a getter material are encapsulated by pore sealing and vitrification. We have found that mixing a radionuclide-loaded getter material with a certain amount of Na-silicate solution can effectively (>90%) seal the nanopores in the material (Fig. 9), thus enhancing radionuclide retention during subsequent vitrification of the material. No significant I loss was observed during vitrification if nanoporous alumina is used as an iodine getter.

A pore-sealed material is finally mixed with a glass-forming frit and vitrified to form a glass-ceramic waste form. We have tested six commercially available frits for their ability to isolate radionuclides. We have found that Ferro frit “510” – a lithium borosilicate material – produces the best result in terms of waste form durability. Figure 10 shows some of glass-ceramic waste forms produced using the proposed nano-immobilization and nano-encapsulation technique. In these waste forms, radionuclide nanoparticles are embedded in either amorphous or crystalline matrix (Fig. 9).

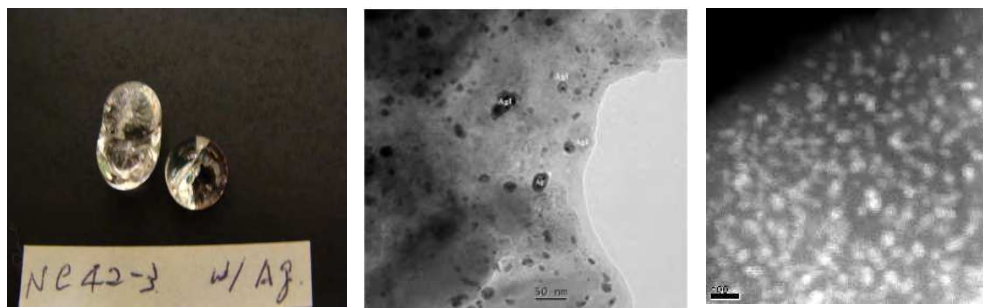


Fig. 10. Glass-ceramic waste forms produced using the proposed nano-scale encapsulation technique. Nanoparticles embedded: left – AgI-embedded glass –ceramic waste form; middle – TEM image of AgI-waste form; right – image of Bi-Tc waste form. Re is used as analog to Tc.

Furthermore, as shown in Table 4, with the fixation and encapsulation methods developed for this work, the loss of iodine during the conversion of an iodine-loaded nanoporous material into a waste form is minimal even at 1100 °C. It is clear that nanoporous structures not only enhance I sorption but also help to retain I during calcination (Table 5).

Glass sample	[I] in the ceramic-glass, ppm	[I], normalized to mass (g) of mesoporous alumina, ppm	vitrification temperature, °C	Iodine loss % during vitrification*
NC48-1+ "510"	429	7064	1100	32
NC48-2 + "510"	915	15067	1100	0
NC48-1 + "XF140-2"	698	11494	1100	0
NC48-2 + "XF140-2"	1069	17603	1100	0
NC52-2 + "3225"	617	9872	1100	5
NC52-2 + "CS749"	570	9120	1100	12
NC67-7	748	11968	1200	0
NC67-6	243	3880	1100	63
iso-750	855	13680	750	0
iso-800	649	10384	800	0
iso-850	659	10544	850	0
iso-900	706	11296	900	0
* Non-zero numbers are due to the heterogeneity of samples.				

Table 4. Iodine loadings on glass-ceramic materials synthesized with various glass forming frits under different process conditions

Material	I sorption (ppm)	% of I lost during fixation	% of I lost during vitrification
Alumina particles	98	Not tested	Not tested
Activated alumina particles	8700	45	65
Nanoporous alumina	25000	0	0

Table 5. Effects of nanoporous structures on I sorption and retention by alumina materials

6. Leaching tests of nanocomposite waste forms

The obtained nanocomposite waste forms were subjected to short-term leaching tests in deionized water. The results are summarized in Table 6. Three observations can be made from the table. First, nanoporous alumina (m-Al-I) fixed with potassium silicate provides the best performance in the leaching tests. Second, a material with no Ag incorporated performs better than the same materials fixed with silver. Therefore, silver may not be necessary for iodine immobilization in a glass-ceramic waste form. Third, there exists an optimal temperature for vitrification. This temperature is about 850-950 °C, which is lower than that used for glass formation (generally > 1100 °C). It is likely that the formation of nano-scale crystalline mineral phases at the optimal temperature may enhance waste form durability, which seems consistent with the high temperature X-ray diffraction (HTXRD) analysis (Fig. 11).

Material	pH-end	Iodine loss, %	vitrification T, °C	[SiO ₂], ppm	composition
First leaching test (LA)					
LA-1	9.29	14.5	1100	not analyzed	m-Al-I+Na ₄ SiO ₄ + "510"
LA-2	9.50	27.4	1100	not analyzed	m-Al-Ag-I+Na ₄ SiO ₄ + "510"
LA-3	8.18	38.5	1100	not analyzed	m-Al-I+Na ₄ SiO ₄ + "XF140-2"
LA-4	8.22	33.3	1100	not analyzed	m-Al-Ag-I+Na ₄ SiO ₄ + "XF140-2"
m-Al-I/silver composite					
LB-1	8.40	37.4	1100	44	3225+NC52-2(vit),
LB-2	8.39	19.6	1100	44	CS749+NC52-2(vit)
LB-3	10.31	40.6	1100	717	m-Al-I + Na ₄ SiO ₄
LB-4	10.66	29.6	1100	664	m-Al-I + Na ₄ SiO ₄
LB-5	8.02	40.6	1100		m-Al-I+Na ₄ SiO ₄ +SiO ₂ +B ₂ O ₃
LB-6	8.28	15.9	1200	27	m-Al-I+Na ₄ SiO ₄ +SiO ₂
m-Al-I samples w/o silver					
LC-1	10.30	5.8	750		750 C. m-Al-I+Na ₄ SiO ₄ + "510" frit
LC2	10.12			1666	750 C. m-Al-I+Na ₄ SiO ₄ + "510" frit
LC-3	9.86	7.8	800	1034	800C. m-Al-I+Na ₄ SiO ₄ + "510" frit
LC-4	9.89			1013	800C. m-Al-I+Na ₄ SiO ₄ + "510" frit
LC-5	9.49	20.9	850	278	850C. m-Al-I+Na ₄ SiO ₄ + "510" frit
LC-6	9.52			419	850C. m-Al-I+Na ₄ SiO ₄ + "510" frit
LC-7	9.17	29.4	900	250	900C.m-Al-I+Na ₄ SiO ₄ + "510" frit
LC-8	9.18			213	900C. m-Al-I+Na ₄ SiO ₄ + "510" frit
m-Al-I samples fixed with potassium silicate					
LD-1	9.96	0.0	750	1444	750 C. m-Al-I+Na ₄ SiO ₄ + "510" frit
LD-2	10.02	0.0		2145	750 C. m-Al-I+Na ₄ SiO ₄ + "510" frit
LD-3	9.74	0.0	800	987	800C. m-Al-I+Na ₄ SiO ₄ + "510" frit
LD-4	9.52	0.0		497	800C. m-Al-I+Na ₄ SiO ₄ + "510" frit
LD-5	9.20	0.0	850	206	850C. m-Al-I+Na ₄ SiO ₄ + "510" frit
LD-6	9.15	0.0		174	850C. m-Al-I+Na ₄ SiO ₄ + "510" frit
LD-7	8.68	13.5	900	279	900C.m-Al-I+Na ₄ SiO ₄ + "510" frit
LD-8	8.94	7.6		279	900C. m-Al-I+Na ₄ SiO ₄ + "510" frit

Table 6. Summary of leaching tests

The leaching rate of the waste form depends on the stability of both radionuclide-bearing nanocrystallites and their surrounding matrix. HTXRD analyses indicate that at a relatively low sintering temperature, e.g., between 750-800 °C, several crystalline phases appear (Fig. 11). The leaching test result indicates that glass-ceramic waste forms vitrified at 750 °C seem to have the lowest iodine loss during leaching. This may be due to the high content of

crystalline quartz (possibly as the embedding matrix) as well as the presence of crystalline lithium silicate. In the case of the glass ceramic sample containing Ag, nanocrystals of AgI are observed to be embedded in crystalline quartz. At a higher vitrification temperature, iodine anions are expected to distribute more uniformly in the resulting waste form, probably “dissolved” in the glass matrix, thus transitioning from nano-scale radionuclide encapsulation to traditional mineral structural incorporation and resulting in less resistant waste forms.

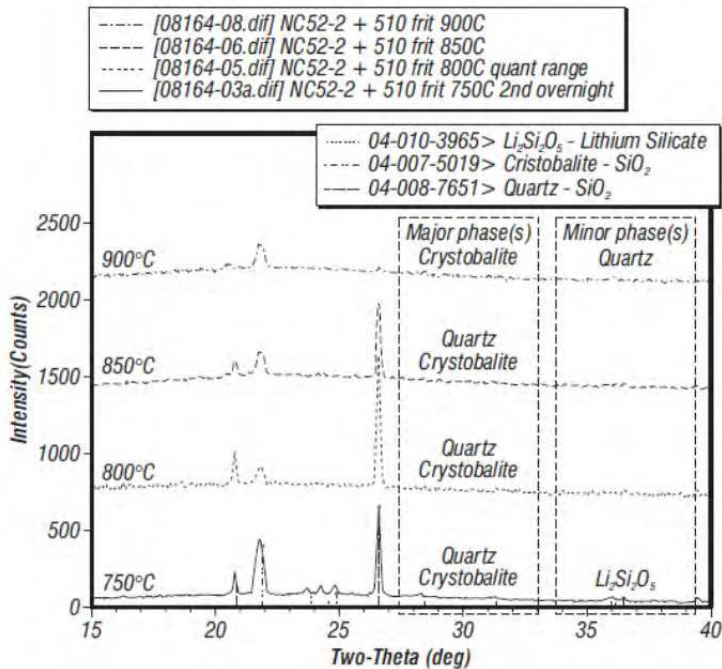


Fig. 11. XRD patterns of glass-ceramic waste forms showing the crystallinity change with increasing vitrification temperatures. Quartz, cristobalite and lithium silicate occur in the 750 °C sample; these phases disappear at 900 °C as the amorphous phase becomes more dominant.

7. Development of high performance adsorbents by molecular design

Adsorption isotherms were simulated using the sorption module of the Materials Studio software suite (Allen and Tildesley, 1987; Frenkel and Smith, 2002). This software suite allows for simulation of sorption isotherms under a wide variety of conditions (temperature and pressure), and has the capability of handling multiple components simultaneously (e.g. I_2 and H_2O). The parameters for a typical isotherm simulation at 363 K use the Metropolis algorithm (Metropolis et al., 1953), with 1.0×10^5 equilibration steps, and 5×10^5 production steps. Electrostatic summations were treated according to the Ewald method (0.001 kcal/mol accuracy) while van der Waals summations were treated with an atom based method (cubic spline cutoff of 12.5Å).

Sorption studies have included γ -alumina (Al_2O_3), and quartz (SiO_2). The isotherms which included simultaneously both I_2 and H_2O were for direct comparison against relative humidity experimental data (Fig. 7). Parameters for γ - Al_2O_3 are Al: $\sigma = 2.898 \text{ \AA}$, $\epsilon = 0.4916 \text{ kcal/mol}$; O: $\sigma = 3.627 \text{ \AA}$, $\epsilon = 0.0784 \text{ kcal/mol}$; while the parameters for silica: Si: $\sigma = 4.295 \text{ \AA}$, $\epsilon = 0.3000 \text{ kcal/mol}$; O: $\sigma = 3.511 \text{ \AA}$, $\epsilon = 0.1554 \text{ kcal/mol}$. Since we use Grand Canonical Monte Carlo (GCMC) methods, the sorbate and sorbent models are static, bonding terms need not be included in the force field description.

Because of the large atomic radii of iodine and its ability to become polarized, we have opted to use force-field parameters that mimic this molecular phenomenon. Lennard-Jones 6-12 parameters were used for I_2 ($\sigma = 2.376 \text{ \AA}$; $\epsilon = 35.56 \text{ kcal/mol}$) (Kornweitz and Levine, 1998); however, the individual iodine atoms of I_2 were artificially charged ($\delta^\pm = \pm 0.366 e$) (Pasternak et al., 1977) such that molecular neutrality was maintained but a dipole is established (Fig. 12). The result is a sorption analyte which accounts for the molecular polarization of I_2 when it interacts with another atom or surface.

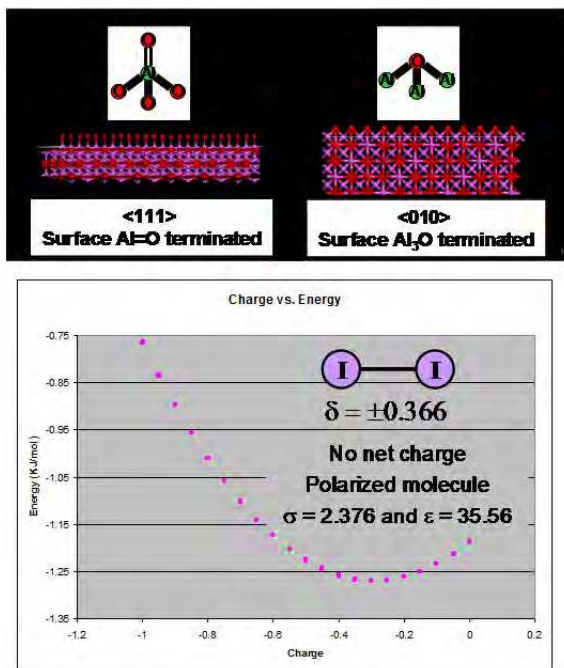


Fig. 12. Model system for iodine sorption on γ -alumina

Comparison of 363K I_2 isotherms between γ -alumina and silica indicate a more significant uptake for the alumina case (Fig. 13). This is consistent with experimental observations that mesoporous silica has a low sorption capability for iodine (Fig. 7). In addition to the maximum uptake capacity, the shape of the isotherm also indicates that the energetics is slightly more favorable in the alumina case. When we compare I_2 uptake versus relative humidity, we can clearly see that increasing the relative humidity reduces the capacity of each material to adsorb molecular I_2 by roughly 50%. This suggests that the I_2 and H_2O are

competing for the same surface adsorption sites and that there are no synergistic effects to consider, which was confirmed by our experimental observations (Fig. 7).

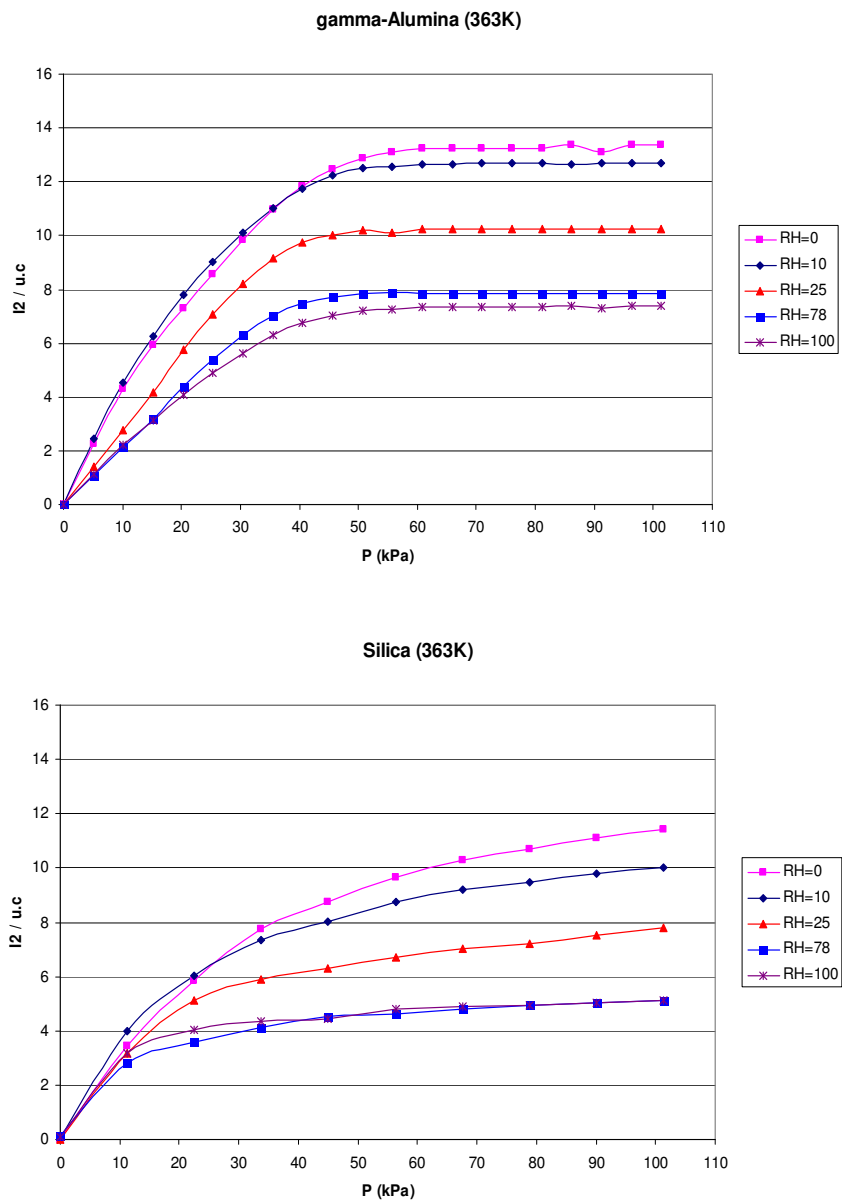


Fig. 13. Molecular dynamic calculations for iodine sorption on alumina and silica surfaces at various relative humidity

The surfaces of these two materials can be terminated structurally in several ways and this could account for the isotherm differences. The first is termination through a single oxygen atom bonded to a single metal (Si or Al) atom ($M=O$) which produces a surface with a significant regular nanostructures. The second possibility is termination by a single oxygen atom bound to three metal (Si or Al) atoms (M_3O) that produces a very uniform surface with little variation in the local nanostructure. In gamma-alumina the predominant surface termination motif is $Al=O$ and not Al_3O and our model reflects this preference. Whereas in silica, the predominant termination motif is considered Si_3O rather than $Si=O$ and our model also reflects this termination preference. This variation in local surface structure could potentially account for the differences we see in the isotherms; however, further simulations (specifically of the $Si=O$ terminated silica) are necessary to prove this hypothesis.

To investigate the effect of space confinement on gaseous radionuclide adsorption, a GCMC simulation was performed for a nanopore represented by two parallel γ -alumina (Al_2O_3) $\langle 111 \rangle$ surfaces. The coordinate perpendicular to the planar walls was changed from 1.5 to 4 nm to simulate different pore sizes. The simulation result for I_2 sorption is shown in Figure 14. Over the pore size range studied, the pore size from 2.5 to 3.0 nm seems to have optimal sorption performance. This result needs to be confirmed by experiments.

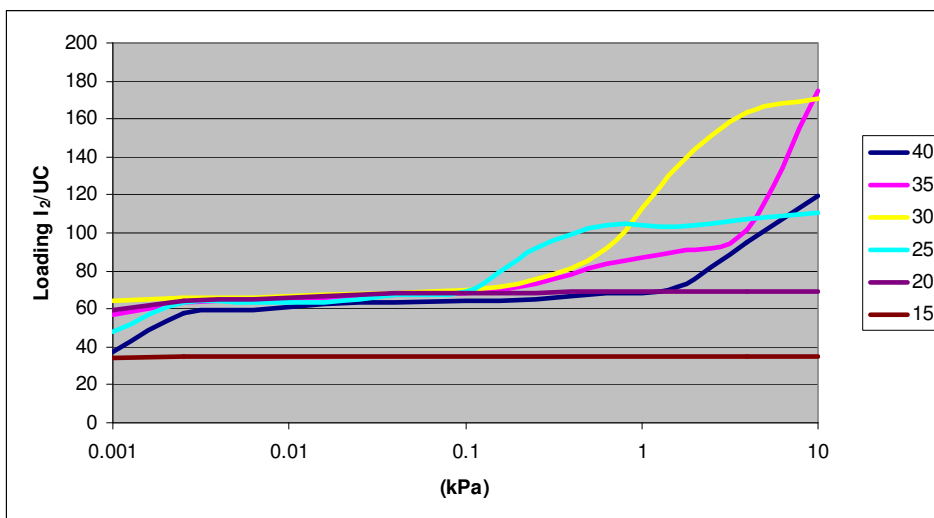


Fig. 14. GCMC adsorption isotherms for iodine sorption onto alumina nanopore surfaces as a function of iodine vapour pressure and pore size. Numbers in the labels are pore sizes in Å.

A GCMC simulation was also performed to investigate the possibility of improving material sorption performance through surface modifications. In the study shown in Figure 15, 60% of oxygen atoms on alumina surface were replaced with F atoms. The simulation result for iodine sorption onto the fluorinated surface is shown in Figure 16. The fluorinated surface appears to have enhanced the attraction of the I_2 molecules to the surface. Based on this result, a technique to graft fluorine functional groups onto nanoporous alumina surfaces is currently under development.

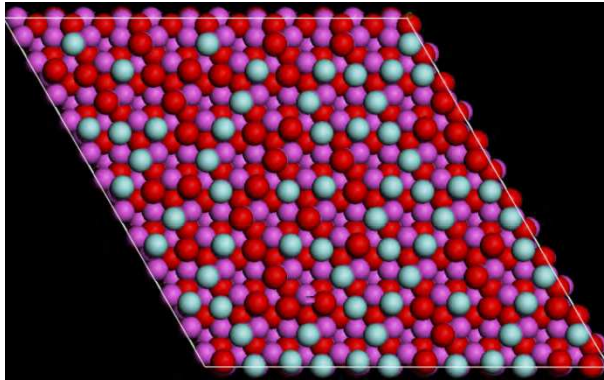


Fig. 15. Plane view of 60% fluorinated alumina surface. Turquoise balls are F, Red = O and Magenta = Al.

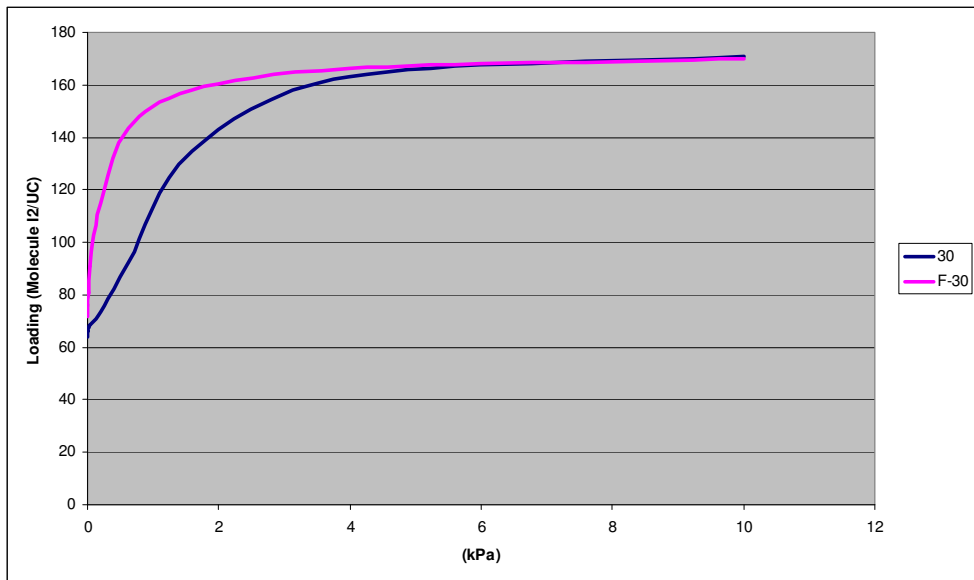


Fig. 16. GCMC simulation result for iodine adsorption onto fluorinated alumina surface. The red curve shows the iodine sorption onto the 60% fluorinated alumina surface.

8. Conclusions

We have proposed a new paradigm for the development of a next generation of high-performance radionuclide adsorbent materials for nuclear waste reprocessing and disposal. Based on this new concept, we have developed a suite of inorganic nanocomposite materials (SNL-NCP) that can effectively entrap various radionuclides, especially for ^{129}I and ^{99}Tc . In particular, these materials have high sorption capabilities for iodine gas. After the sorption of radionuclides, these materials can be directly

converted into nanostructured waste forms. This new generation of waste forms incorporates radionuclides as nano-scale inclusions in a host matrix and thus effectively relaxes the constraint of crystal structure on waste loadings. Therefore, the new waste forms have an unprecedented flexibility to accommodate a wide range of radionuclides with high waste loadings and low leaching rates.

We have developed a general route for synthesizing nanoporous metal oxides from inexpensive inorganic precursors. A large set of nanocomposite materials have been synthesized and characterized with XRD, BET, and TEM. These materials have been tested for their sorption capabilities for radionuclide I and Re (as an analog to Tc). The results have confirmed that nanoporous Al oxide and its derivatives have high I sorption capabilities due to the combined effects of surface chemistry and nanopore confinement. We have developed a suite of techniques for the fixation of radionuclides in metal oxide nanopores. The key to this fixation is to chemically convert a target radionuclide into a less volatile or soluble form. We have also developed a technique to convert a radionuclide-loaded nanoporous material into a durable glass-ceramic waste form through calcination. We have shown that mixing a radionuclide-loaded getter material with a Na-silicate solution can effectively seal the nanopores in the material, thus enhancing radionuclide retention during waste form formation. Our leaching tests have demonstrated the existence of an optimal vitrification temperature for the enhancement of waste form durability. Our work also indicates that silver may not be needed for I immobilization and encapsulation. Molecular dynamic modeling results help clarify the control of surface structure and surface chemistry on iodine sorption onto SNL-NCP materials and thus provide a guide for future improvements to the materials.

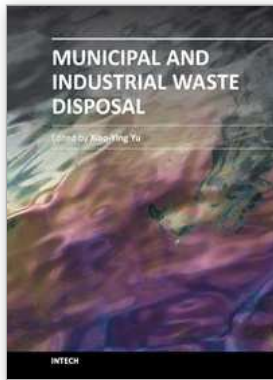
9. Acknowledgment

Sandia is a multiprogram laboratory operated by Sandia Corporation, a Lockheed Martin Company for the United States Department of Energy's National Nuclear Security Administration under contract DE-AC04-94AL85000. This work is supported by DOE Sandia LDRD Program. We thank C. Jeffrey Brinker, Yongliang Xiong, Kathleen Holt, Nathan Ockwig, Mark A. Rodriquez, Denise N. Bencoe, Hernesto Tellez, Jessica Nicole Kruichak, Rigney Turnham, and Andrew Wilson Murphy for their help with the work.

10. References

- Allen, M. P. & Tildesley, D. J. (1987) *Computer Simulation of Liquids*. Clarendon Press, Oxford.
- Bodansky, D. (2006) Reprocessing spent nuclear fuel, *Physics Today*. December 2006, pp. 80-81.
- Ewing, R. C. (2006) The nuclear fuel cycle: A role for mineralogy and geochemistry, *Elements*. Vol. 2, pp. 331-334.
- Fortner, J. A.; Kropf, A. J.; Finch, R. J.; Bakel, A. J.; Hash, M. C. & Chamberlain, D. B. (2002) Crystal chemistry of uranium (V) and plutonium (IV) in a titanate ceramic for disposition of surplus fissile material, *J. Nuclear Mater.* Vol. 304, pp. 56-62.
- Frenkel, D. & Smith, B. (2002) *Understanding Molecular Simulation: From Algorithms to Applications, 2nd Edition*. Academic Press, San Diego.

- Gombert, D. (2007) *Appendixes for Global Nuclear Energy Partnership Integrated Waste Management Strategy Waste Treatment Baseline Study*. Idaho National Laboratory, GENP-WAST-WAST-AI-RT-2007-000324.
- Grambow, B. (2006) Nuclear waste glasses - How durable? *Elements*, Vol. 2, pp. 357-364.
- Jubin, R. T. (1994) *The Mass Transfer Dynamics of Gaseous Methyl-Iodide Adsorption by Silver-Exchanged Mordenite*. Oak Ridge National Laboratory, ORNL-6853.
- Kato, H.; Kato, O. & Tanabe, H. (2002) *Review of Immobilization of Techniques of Radioactive Iodine for Geological Disposal*. JAERI-Conf 2002-004.
- Kornweitz, H. & Levine, R. D. (1998) Formation of molecular iodine in high-energy four-center CH₃I+CH₃I collisions, *Chem. Phys. Lett.* Vol. 294, pp. 153-161.
- Lee, J. Y.; Olson, D. H.; Pan, L.; Emge, T. J. & Li, J. (2007) Microporous metal-organic frameworks with high gas sorption and separation capacity, *Advanced Functional Materials*, Vol. 17, 1255-1262.
- Metropolis, N.; Rosenbluth, A. W.; Rosenbluth, M. N.; Teller, A. H. & Teller, E. (1953) Equation of state calculations by fast computing machines, *J. Chem. Phys.* Vol. 21, 1087-1092.
- NEA OECD (2006) *Advanced Nuclear Fuel Cycles and Radioactive Waste Management*. NEA No. 5990.
- Pasternak, A.; Anderson, A. & Leech, J. W. (1977) Bond charge model for lattice-dynamics of iodine, *J. Phys. C: Solid State Phys.* Vol. 10, pp. 3261-3271.
- Peters, M. & Ewing, R. C. (2007) A science-based approach to understanding waste form durability in open and closed nuclear fuel cycles, *J. Nuclear Materials*. Vol. 362, pp. 395-401.
- Rovnyi, S. I.; Pyatin, N. P. & Istomin, I. A. (2002) Catching of I-129 during processing of spent nuclear fuel from power plants, *Atomic Energy*. Vol. 92, pp. 534-535.
- Stephenson, D.J.; Fairchild, C.I.; Buchan, R.M., & Dakins, M.E. (1999) A fiber characterization of the natural zeolite, mordenite: A potential inhalation health hazard, *Aerosol Science and Technology*. Vol. 30, pp. 467-476.
- Sudik, A. C.; Côté, A. P.; Wang-Foy, A. G.; O'Keeffe, M. & Yaghi, O. M. (2006) A metal-organic framework with a hierarchical system of pore and tetrahedral building blocks, *Angewandte Chemie*, Vol. 45, 2528-2533.
- Wang, Y. & Gao, H. (2006) Compositional and structural control on anion sorption capability of layered double hydroxides (LDHs), *J. Colloid Interface Sci.* Vol. 301, pp. 19-26.
- Wang, Y.; Bryan, C.; Gao, H.; Pohl, P.; Brinker, C. J.; Yu, K.; Xu, H.; Yang, Y.; Braterman, P. S. & Xu, Z. (2006) *Potential Applications of Nanostructured Materials in Nuclear Waste Management*. Sandia National Laboratories, Albuquerque, NM. SAND2003-3313.
- Wang, Y.; Bryan, C.; Xu, H. & Gao, H. (2003) Nanogeochemistry: Geochemical reactions and mass transfers in nanopores, *Geology*, Vol. 31, 387-390.
- Wang, Y.; Gao, H.; Yeredla, R.; Xu, H. & Abrecht, M. (2006) Control of surface functional groups on pertechnetate sorption on activated carbon, *J. Colloid Interface Sci.*, 305, 209-217.
- Xu, H. & Wang, Y. (2000) Crystallization sequence and microstructure evolution of Synroc samples crystallized from CaZrTi₂O₇ melts, *J. Nuclear Mater.* Vol. 279, pp. 100-106.



Municipal and Industrial Waste Disposal

Edited by Dr. Xiao-Ying Yu

ISBN 978-953-51-0501-5

Hard cover, 242 pages

Publisher InTech

Published online 11, April, 2012

Published in print edition April, 2012

This book reports research findings on several interesting topics in waste disposal including geophysical methods in site studies, municipal solid waste disposal site investigation, integrated study of contamination flow path at a waste disposal site, nuclear waste disposal, case studies of disposal of municipal wastes in different environments and locations, and emissions related to waste disposal.

How to reference

In order to correctly reference this scholarly work, feel free to copy and paste the following:

Yifeng Wang, Huizhen Gao, Andy Miller and Phillip Pohl (2012). A New Generation of Adsorbent Materials for Entrapping and Immobilizing Highly Mobile Radionuclides, *Municipal and Industrial Waste Disposal*, Dr. Xiao-Ying Yu (Ed.), ISBN: 978-953-51-0501-5, InTech, Available from: <http://www.intechopen.com/books/municipal-and-industrial-waste-disposal/a-new-generation-of-adsorbent-materials-for-entrapping-and-immobilizing-highly-mobile-radionuclides>

INTECH

open science | open minds

InTech Europe

University Campus STeP Ri
Slavka Krautzeka 83/A
51000 Rijeka, Croatia
Phone: +385 (51) 770 447
Fax: +385 (51) 686 166
www.intechopen.com

InTech China

Unit 405, Office Block, Hotel Equatorial Shanghai
No.65, Yan An Road (West), Shanghai, 200040, China
中国上海市延安西路65号上海国际贵都大饭店办公楼405单元
Phone: +86-21-62489820
Fax: +86-21-62489821

© 2012 The Author(s). Licensee IntechOpen. This is an open access article distributed under the terms of the [Creative Commons Attribution 3.0 License](#), which permits unrestricted use, distribution, and reproduction in any medium, provided the original work is properly cited.